ARTICLE

Experimental and Density Functional Theory Calculation Studies on Raman and Infrared Spectra of 1,1′-Binaphthyl-2,2′-diamine

Zhen-lin Zhang[a], Wen-lou Wang[a,b], Shi-lin Liu[a], Dong-ming Chen[a]*

a. Department of Chemical Physics, University of Science and Technology of China, Hefei 230026, China

b. National Synchrotron Radiation Laboratory, University of Science and Technology of China, Hefei 230029, China

(Dated: Received on June 1, 2016; Accepted on June 3, 2016)

The IR absorption, visible excited normal Raman, and UV-excited near-resonant Raman (UVRR) spectra of 1,1′-binaphthyl-2,2′-diamine (BINAM) were measured and analyzed. Density functional theory calculations were carried out to investigate its vibrational frequencies, infrared absorption, normal Raman, and near-resonance Raman intensities. The observed Raman and IR bands of BINAM were assigned with respect to the local vibrations of substituted 2-naphthylamine. Several Raman bands of BINAM were found selectively enhanced in the UVRR in comparison with the normal Raman spectrum. Possible excited state geometry distortion was discussed based on the resonance Raman intensity analysis.

Key words: 1,1′-Binaphthyl-2,2′-diamine, Resonance Raman, Infrared, Density functional theory, Molecular vibrations

I. INTRODUCTION

The axially chiral binaphthyl compounds play a crucial role in constructing new stable chiral structures as well as in developing effective asymmetric organocatalysts [1−18]. Various spectroscopic methods have been used to explore the structures and properties of the binaphthyl compounds, especially the 1,1′-binaphthyl-2,2′-diol, in the past several decades [19−31]. For example, Nogueira *et al.* measured the surface-enhanced Raman spectrum (SERS) of 1,1′-binaphthyl-2,2′-diol on silver colloids and proposed the empirical assignments for the observed SERS bands [19]. In Ref.[20], the vibrational circular dichroism (VCD) spectrum of 1,1′-binaphthyl-2,2′-diol was studied and density functional theory (DFT) calculations were carried out to assign the VCD bands. With ultralow-frequency Raman technique, Chang *et al.* studied the polymorphic transformation of crystalline binaphthyls [21]. Li *et al.* studied the normal and UV near-resonant Raman (UVRR) spectra of 1,1′-binaphthyl-2,2′-diol in basic solution and assigned the observed Raman bands on the basis of the DFT-calculations [22]. Vibrational spectroscopy and DFT calculations have also been extensively used to investigate the chiral conformational stability of the binaphthyl compounds [23−25]. The solutions of 1,1′-binaphthyl-2,2′-diol have also been studied by the sum-frequency generation (SFG) spectroscopies [26−30]. Recently, Liégeois have conducted a comprehensive theoretic study on the polarized Raman and vibrational Raman optical activities (VROA) of a series of 2,2′-substituted binaphthyl compounds [31].

Among various binaphthyl compounds, the 1,1′-binaphthyl-2,2′-diamine (BINAM) derivatives have been found highly useful in developing new asymmetric catalysts [7−18]. For example, Guillena *et al.* have synthesized a series of BINAM-prolinamides and used them as catalysts in several organic reactions, such as the direct aldol condensation between aldehydes and aliphatic ketones [8−12]. Starting from BINAM, Duan *et al.* have obtained a novel axially chiral Rh-complex and applied it in the Rh-catalyzed enantioselective hydrosilylation of methyl ketone [13]. By using BINAM-derived phosphoric acids, Nelson *et al.* recently developed a chiral anion phase-transfer stretagy to achieve highly enantioselective α-amination of carbonyl compounds [15]. Barbas group has discovered a highly efficient organocatalytic domino approach for the direct construction of bispirooxindole derivatives with excellent stereocontrol by employing an organocatalyst containing a BINAM skeleton [17].

On the other hand, despite of its significance in asymmetric catalysis, the spectroscopic properties of BINAM have not been well studied. To the best of our knowledge, the experimental and theoretical study of Raman and IR spectra of BINAM has never been reported. Therefore, the present study was conducted with the intention to provide a detailed vibrational analysis for BINAM by conjunct investigation of IR/Raman experiments and DFT calculations. The assignments of the

*Author to whom correspondence should be addressed. E-mail: dmchen@ustc.edu.cn

observed IR and Raman bands have been proposed based on the local vibrations of substituted 2-naphthylamine. The UVRR spectrum of BINAM was also measured and its resonant enhancement pattern was discussed and used to analyze the possible distortion of the excited state structure.

II. EXPERIMENTAL AND COMPUTATIONAL METHODS

1,1′-binaphthyl-2,2′-diamine (>99%) was purchased from Alfa Aesar and was used without further purification. UV-Vis absorption spectra were measured with a 5 mm light-path quartz cell at room temperature using Shimadzu UV-2401PC spectrometer. Raman spectra were recorded on a LABRAM-HR 800 micro-Raman spectrometer equipped with an air-cooled CCD detector, a notch filter, and a 600 grooves/mm grating for the visible excitation and a 2400 grooves/mm grating for UV. The 325 nm line of a He-Cd laser and the 488.0 nm line of an Ar ion laser were used as the excitation sources with the power 3.5 and 5 mW, respectively, on the sample. The collection time of the CCD detector was 40 s for Raman measurements. In order to minimize any damage of the sample due to the prolonged exposure to laser radiation, the BINAM solid sample was mixed with KBr powder in a weight ratio of 1:10 and pressed into a disc of 1 cm diameter, which was placed on a rotating holder during Raman measurements. IR spectrum of BINAM was measured on a Nicolet 6700 FT-IR spectrometer as KBr pallet.

DFT calculations were carried out using Becke's three-parameter hybrid functional (referred as B3LYP) [32, 33], which has been proven to be suitable for studying the structures and properties of binaphthyl systems [22, 25, 29−31]. In order to reduce computational cost, initial searching of steady structure of the studied molecule was carried out by geometry optimization with relative small basis sets, 6-31G, without any symmetry constraint. The obtained structures were then used for the final optimization using 6-311++G(d,p) basis sets with suitable symmetry (C_2 point group) constraint. Analytic frequency calculations (using B3LYP/6-311++G(d,p)) at the optimized structure were done to confirm the optimized structures to be an energy minimum and to obtain the theoretical vibrational spectra. Due to the neglect of the anharmonicity and the incomplete basis sets, the DFT calculations tend to slightly overestimate the vibrational frequencies. These systematic discrepancies between the computed and experimental frequencies can be corrected by scaling the calculated frequencies with a single factor of 0.98, which has been found to be appropriate for the planar conjugate systems [34, 35]. Assignment of individual vibrational frequency was carried out by inspecting the calculated Cartesian displacements of the corresponding normal mode. Electronic absorption spectrum of BINAM was theoretically studied with TDDFT calculations [36−38]. The simulation of UV-resonance Raman spectrum was carried out with frequency-dependent polarizability using coupled-perturbation theory (CPHF). All DFT/TDDFT calculations were performed with the Gaussian 09 program suite [39].

TABLE I Selected structural parameters of BINAM calculated with B3LYP/6-311++G(d,p). Distance in Å and angles or dihedral angles in (°).

Bond	Distance	Bond	Angles
C1−C2	1.394	C1−C2−C3	119.9
C2−C3	1.425	C2−C3−C4	121.0
C3−C4	1.367	C3−C4−C10	121.1
C4−C10	1.419	C10−C5−C6	121.0
C5−C10	1.417	C5−C6−C7	119.6
C5−C6	1.375	C6−C7−C8	120.8
C6−C7	1.413	C7−C8−C9	121.1
C7−C8	1.376	C8−C9−C1	122.2
C8−C9	1.423	C1−C9−C10	120.0
C9−C10	1.432	C2−C1−C9	119.5
C9−C1	1.431	C2−C1−C1′−C2′	91.4
C2−N11	1.398	C2−C1−C1′−C9′	88.4
C1−C1′	1.497		

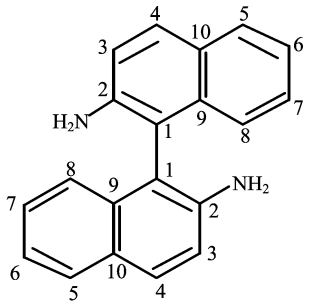

FIG. 1 Structural sketch of BINAM with the atomic labels.

III. RESULTS AND DISCUSSION

A. Ground-state geometries and UV-visible absorption spectrum

Table I lists the bond lengths, bond angles and dihedral angles of BINAM optimized with B3LYP/6-311++G(d,p). Figure 1 shows the structural sketch and atomic labels of BINAM used in this work. B3LYP/6-311++G(d,p) calculations indicate that the two naphthyl rings of BINAM molecule are almost perpendicular with each other. The dihedral angle between the two naphthyl groups is about 91.4°. The C1−C2, C2−C3, and C9−C10 distances of BINAM are calculated to be 1.394, 1.425, and 1.432 Å, respectively, while the C1−C9 distance is found to be 1.431 Å. The C−N bond length of BINAM is 1.398 Å.

DOI:10.1063/1674-0068/30/cjcp1606118

TABLE II Frontier orbital energies of BINAM by B3LYP/6-311++G(d,p) calculations.

Orbital	Energy/eV	Orbital
34b	−8.205	HOMO−6
36a	−7.690	HOMO−5
35b	−7.484	HOMO−4
37a	−6.357	HOMO−3
36b	−6.354	HOMO−2
38a	−5.540	HOMO−1
37b	−5.492	HOMO
39a	−1.253	LUMO
38b	−1.179	LUMO+1
40a	−0.428	LUMO+2
39b	−0.323	LUMO+3
41a	−0.301	LUMO+4
40b	−0.094	LUMO+5
41b	−0.019	LUMO+6

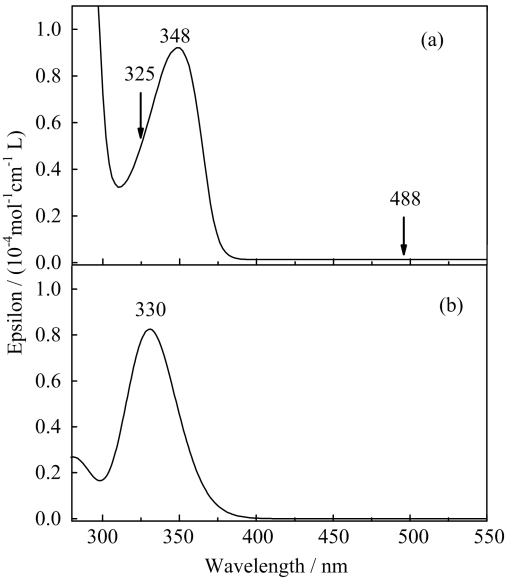

FIG. 2 (a) UV-Vis absorption spectra of BINAM measured in CH_2Cl_2 solution. The arrows mark the wavelength positions of excitation lines for Raman experiments. (b) UV-Vis absorption spectra of BINAM calculated by TD-B3LYP/6-311++G(d,p) calculation.

Figure 2(a) displays the UV-Vis absorption spectrum of R-BINAM dissolved in CH_2Cl_2, which shows a quite broad peak with the absorption maximum at 348 nm. Figure 2(b) gives the theoretical spectrum of BINAM calculated with TD-B3LYP/6-311++G(d,p), where a band-width of 2600 cm^{-1} (0.322 eV) was utilized for each electronic transition in the spectral simulation. Table II tabulates the calculated orbital energies and symmetries of frontier molecular orbitals of BINAM, and Table III lists the calculated excitation energies and oscillator strengths of BINAM calculated with TD-B3LYP/6-311++G(d,p). Table III also gives the weights of major configurations for each excited state. According to the TD-B3LYP calculations, the near-UV absorption of BINAM are contributed from the transitions from the ground state to 1^1B, 1^1A, 2^1B, and 2^1A states, with 1^1B, 2^1B, and 2^1A being of relatively large oscillator strengths. As shown in Table III, the transition energies of these four states are quite close with each other, while they are well separated from higher excited states (3^1B, *etc.*). Thus the observed broad 348 nm peak in Fig.2(a) can be attributed to the overlap of the 1^1B, 2^1B, and 2^1A states.

B. Vibrational spectra

1. Infrared absoption spectrum

BINAM has 38 atoms and 108 degrees of internal freedom, which, according to the C_2 symmetry, can be classified as Γ=55A+53B. According to the vibrational selection rules, all of these modes are active for both IR and Raman transitions. As the two naphthyl rings of BINAM are nearly perpendicular to each other, most vibrational modes of BINAM can be considered as the in-phase and out-of-phase combinations of the corresponding local vibrations of two isolated naphthylamine groups. The molecular vibrations of naphthalene have been studied by Scherer [40], but it is not very useful in helping our vibrational assignments since the substituents in BINAM significantly alter the mode compositions. Therefore, we conducted a supplementary frequency calculation on 1-chloro-2-naphthylamine molecule and used the corresponding modes to describe and classify the normal vibrations of BINAM. In this way, the in-phase or out-of-phase coupling (so called vibrational exciton coupling) of the corresponding local vibrations of two naphthylamine groups generates A and B symmetry blocks of normal modes of BINAM. The calculated atomic Cartesian displacements of 1-chloro-2-naphthylamine are shown in Figs. S1 and S2 in the supplementary materials. Detailed vibrational assignments of BINAM will be discussed in the following parts of the article.

Figure 3 compares the experimental and theoretical IR spectra of BINAM, where the theoretical IR spectrum has been simulated from B3LYP-calculated harmonic frequencies (scaled with 0.98) and intensities. By comparing with the DFT-calculated band positions and intensities, the observed IR bands of BINAM are assigned as listed in Tables IV and V. In the Tables, the mode numbers are according to those of isolated 1-chloro-2-naphthylamine molecule, and the single quotation marks are added after the mode numbers for the B symmetry modes so as to distinct them from the A modes. It is noticed that, while both A and B modes are IR active, B3LYP calculations indicate that most of the strong IR absorptions of BINAM in the high frequency region (950−1600 cm^{-1}) are due to the in-plane

DOI:10.1063/1674-0068/30/cjcp1606118

TABLE III TD-B3LYP calculated excitation energies (ΔE), oscillate strengths (f), and main configurations for the low-lying excited states of BINAM[a].

States	ΔE/eV	f	Assignment[b]
1^1B	3.6101	0.0329	H−1→L+1(−0.22571), H→L(0.66280)
1^1A	3.6341	0.0001	H−1→L(0.57883), H→L+1(−0.40015)
2^1B	3.7780	0.0786	H−1→L+1(0.64609), H→L(0.19733), H→L+2(0.12458)
2^1A	3.7988	0.0213	H−1→L(0.37068), H→L+1(0.55744)
3^1B	4.3556	0.0200	H−3→L+1(0.29032), H−2→L(−0.37381), H−1→L+1(−0.12037), H−1→L+3(0.20274), H→L+2(0.44479)
3^1A	4.3649	0.0098	H−3→L(0.36586), H−2→L+1(−0.29665), H−1→L+2(0.34264), H→L+1(−0.11527), H→L+3(0.34666)
4^1A	4.5005	0.0008	H−1→L+2(0.50277), H→L+3(−0.48816)
4^1B	4.5097	0.0050	H−1→L+3(0.50277), H−1→L+5(−0.11709), H→L+2(−0.42864), H→L+4(−0.14212)

[a] Basis sets: 6-311++G(d,p).
[b] H=HOMO, L=LUMO, *etc.*

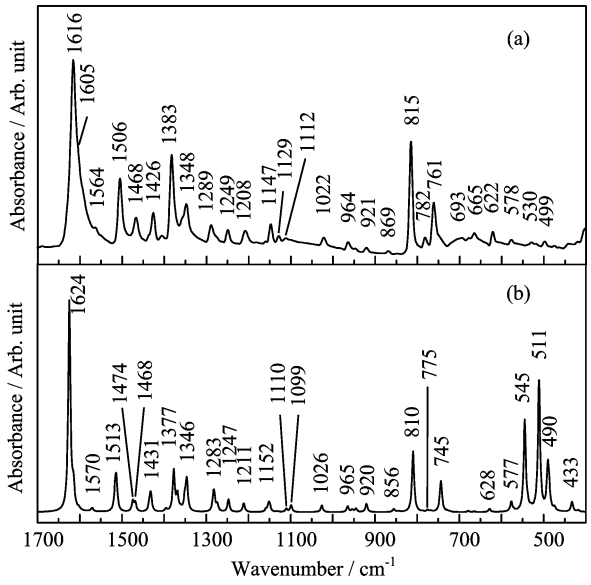

FIG. 3 IR absorption spectra of BINAM (a) experimental (in KBr pellet), (b) calculated with B3LYP/6-311++G(d,p).

naphthyl modes belong to the B symmetry block.

The vibrations in the region 1200−1650 cm^{-1} are mainly due to the C=C stretches of naphthyl rings, and some of which are coupled with the NH_2 scissoring vibrations. The strongest absorption was measured at 1616 cm^{-1}, which is rather broad and can be decomposed into a main band at 1616 cm^{-1} and a shoulder band at 1605 cm^{-1}. DFT-calculations show a very strong IR band at 1624 cm^{-1} and a shoulder band at 1615 cm^{-1}. However, according to calculation the 1624 cm^{-1} band itself is an overlapped band by two normal modes which can be assigned to ν_7 and ν_7' (the C=C stretches of the naphthyl rings), both of which are severely coupled with the NH_2 scissoring vibrations. The shoulder band at 1605 cm^{-1} can be assigned to ν_8', which is calculated at 1615 cm^{-1} and is also severely coupled with the NH_2 scissoring. Other predominant IR absorptions in 1200−1650 cm^{-1} region were measured at 1506, 1468, 1426, 1383, 1348, 1289, 1249, and 1208 cm^{-1}. They are thought to correspond to the calculated bands at 1516/1513 (ν_{10}/ν_{10}'), 1468(ν_{11}'), 1431(ν_{12}'), 1377(ν_{13}'), 1346(ν_{15}'), 1283 (overlapped by ν_{16} and ν_{16}'), 1247(ν_{17}'), and 1211 cm^{-1}(ν_{18}'), respectively.

In the region 950−1200 cm^{-1}, IR bands were observed at 1147, 1129, 1112, 1022, and 964 cm^{-1} and the corresponding absorptions are calculated at 1152 (ν_{20}'), 1110 (ν_{21}), 1099 (NH_2 rocking), 1026 (ν_{22}'), and 965 cm^{-1} (ν_{23}'+NH_2 rocking), respectively, with middle or weak intensities.

In 700−950 cm^{-1} region, IR absorptions were observed at 921, 869, 815, 782, and 761 cm^{-1} and calculated at 920 (ν_{24}'), 856 (γ_4)/855 (γ_4'), 810 (γ_5/γ_5'), 775 (γ_6), and 745/743 cm^{-1} (γ_7/γ_7'), respectively. According to the calculation, most of them are due to the out-of-plane wagging of the hydrogen atoms on the naphthyl rings. In the 400−700 cm^{-1} region, our B3LYP-calculation predicted three strong IR bands at 545 (γ_{10}+NH_2 wagging), 511 (NH_2 wagging+γ_8), and 490 cm^{-1} (ν_{29}+NH_2 wagging) which can be assigned to the in-plane or out-of-plane skeletal deformation of the naphthyl rings together with NH_2 wagging). Experimentally, only weak absorptions were observed probably because of the interference of broad background in the low-frequency region.

2. Normal Raman spectrum excited at 488.0 nm

Figure 4(a) displays the normal Raman spectrum of BINAM in solid discs with 488.0 nm excitation, while the calculated non-resonant Raman is shown in Fig.4(b). The experimentally observed and DFT-

DOI:10.1063/1674-0068/30/cjcp1606118

TABLE IV Observed and calculated vibrational frequencies of BINAM in the range of 1000−1650 cm^{-1}.

Sym.	Calc.[a]	Observed		Assignment[d]
		IR[b]	Raman[b,c]	
A	1625		1618 (s)	ν_7+δ(NH_2 scis.)
B	1624	1616 (s)		ν'_7+δ(NH_2 scis.)
B	1615	1605 (sh)		ν'_8+δ(NH_2 scis.)
B	1602	1595 (sh)		δ(NH_2 scis.)+ν_8
A	1602		1594 (w)	δ(NH_2 scis.)+ν_8
A	1575		1573 (s)	ν_9
B	1570	1564 (w)		ν'_9
A	1516			ν_{10}
B	1513	1506 (vs)		ν'_{10}
A	1474		1476 (s)	ν_{11}
B	1468	1468 (s)		ν'_{11}
A	1434		1439 (s)	ν_{12}
B	1431	1426 (s)	1429 (sh)	ν'_{12}
A	1395		1396(sh)	ν_{13}
B	1377	1383 (vs)		ν'_{13}
A	1368		1381 (vs)	ν_{14}
B	1361		1358 (s)	ν'_{14}
A	1351	1358 (sh)		ν_{15}
B	1346	1348 (s)		ν'_{15}
B	1283	1289 (m)		ν'_{16}
A	1281		1289 (sh, w)	ν_{16}
A	1274		1276 (m)	ν_{17}
B	1247	1249 (m)		ν'_{17}
A	1213		1215 (m)	ν_{18}
B	1211	1208 (m)		ν'_{18}
A	1205		1208 (sh)	ν_{23}
B	1159		1158 (sh, w)	ν'_{19}
A	1158			ν_{19}
B	1152	1147 (m)	1146 (m)	ν'_{20}
A	1149			ν_{20}
A	1110	1129 (w)		ν_{21}
B	1099	1112 (w)	1113 (w)	δ(NH_2 rock.)
A	1040		1046 (w)	δ(NH_2 rock.)+ν_{24}
B	1026	1022 (w)		ν'_{22}
A	1026		1024 (s)	ν_{22}

[a] Calculated with B3LYP/6-311++G(d,p). Frequency scaling factor=0.98.
[b] vs: very strong, s: strong, m: medium; w: weak, vw: very weak, sh: shoulder peak.
[c] From solid Raman spectrum excited at 488 nm.
[d] Mode numbers according to the local modes of 1-chloro-2-naphthylamine (see Fig.S1 and S2 in supplementary materials for details).
ν: bond stretching, δ: naphthyl in-plane bond-angle bending, γ: naphthyl out-of-plane distortion.
NH_2 vibrations: scis.=scissoring, rock.=rocking, wag.=wagging, twist.=twisting.

TABLE V Observed and calculated vibrational frequencies (in cm^{-1}) of BINAM in the range of 400−1000 cm^{-1}.

Sym.	Calculated	Observed		Assignment
		IR	Raman	
B	965	964 (m)		ν'_{23}+δ(NH_2 rock.)
A	954			γ_2
A	945	947 (w)	960 (m)	ν_{24}+γ_3
B	920	921 (w)	922 (w)	ν'_{24}
A/B	856/855	869 (w)		γ_4/γ'_4
A	844		852 (s)	ν_{25}
A/B	810/810	815 (vs)		γ_5/γ'_5
B	787		794 (w)	ν'_{25}+γ'_4
A	775	782 (m)		γ_6
B	768		774 (w)	γ'_6+ν'_{25}
A/B	745/743	761 (vs)		γ_7/γ'_7
B	679	693 (br)		γ'_8
A	677	679 (w)		γ_8
A	665	665 (w)	668 (m)	ν_{27}
B	628	622 (m)		ν'_{27}
A	577	578 (w)	577 (m)	γ_9+ν_{29}
A	545	530 (w)		γ_{10}+γ(NH_2 wag.)
A	530		528 (m)	ν_{28}
B	519	520 (vw)	519 (w)	ν'_{28}
A	511	499 (w)	499 (w)	γ(NH_2 wag.)+γ_8
A	490	475 (vw)	473 (w)	ν_{29}+γ(NH_2 wag.)
B	487	464 (vw)		γ(NH_2 wag.)
B	474	443 (vw)		ν'_{29}+γ'_9
B	433		436 (m)	ν'_{30}+γ'_9
A	433		421 (w)	ν_{30}+γ_{11}

Note: the same as Table IV.

calculated frequencies and assignments of Raman bands of BINAM are listed in Tables IV and V.

In the non-resonance Raman spectrum of BINAM (Fig.4(a)), strong Raman bands were observed at 1618, 1573, 1476, 1439, 1381, 1358, 1024, 852, 668, 577, and 528 cm^{-1}. As shown in Tables IV and V, most of the vibrations of BINAM in the 900−1650 cm^{-1} region are due to the naphthyl in-plane CC stretching and CH bending. In the 1550−1650 cm^{-1} region, three bands were observed at 1618, 1594, and 1573 cm^{-1}, respectively, in the normal Raman spectrum of BINAM. The 1573 and 1618 cm^{-1} bands of BINAM are much stronger than the 1594 cm^{-1} band. Theoretically, B3LYP/6-311++G(d,p) calculations give rise to three bands at 1573, 1602, and 1624 cm^{-1}, respectively, with similar relative intensities to the experiment. According to our DFT calculations, the strong 1573 cm^{-1} band can be attributed to ν_9, the stretching of C2C3/C6C7/C9C10 bonds of the naphthyl rings. On the other hand, the B3LYP/6-311++G(d,p) calculation manifests that the bands at 1602 and 1624 cm^{-1} are as-

DOI:10.1063/1674-0068/30/cjcp1606118

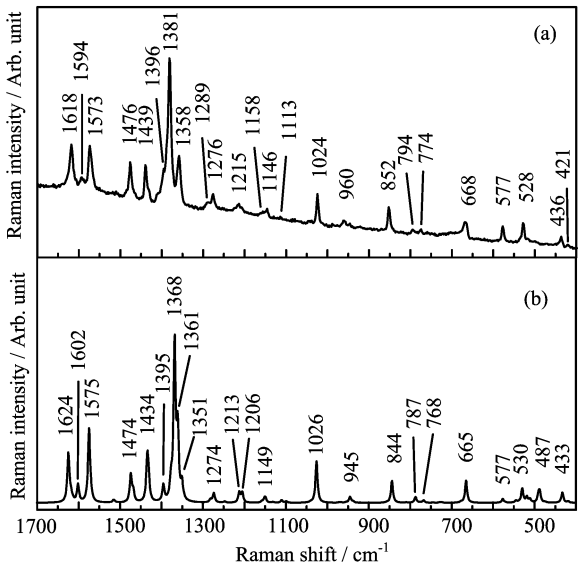

FIG. 4 Normal Raman scattering spectra of BINAM (a) experimental (solid) with the excitation wavelength λ_{ex}=488 nm, (b) calculated with B3LYP/6-311++G(d,p).

sociated mainly with the naphthyl C3C4/C1C2/C5C6 stretching but they also contain significant contributions from NH_2 scissoring. Similar to that observed in IR spectrum, the 1624 cm^{-1} Raman band in Fig.4(b) also comes from two overlapped normal modes, ν_7 and ν_7'. Two strong Raman bands were observed at 1476 and 1439 cm^{-1} (Fig.4(a)), which are thought corresponding to the calculated bands at 1474 (ν_{11}) and 1434 cm^{-1} (ν_{12}). Based on our DFT calculations, these two bands are assigned to the CC stretching of naphthyl ring, and both of them also involves significant contributions from in-plane CCH bending.

With 488 nm excitation, the strongest Raman band of BINAM was observed at 1381 cm^{-1}, and also a strong Raman band at 1358 cm^{-1} was observed at the low-frequency side of the 1381 cm^{-1}band. B3LYP/6-311++G(d,p) calculation of BINAM predicts a very strong Raman at 1368 cm^{-1} (ν_{14}) and two shoulder bands at 1361 (ν_{14}') and 1351 cm^{-1} (ν_{15}), respectively, at low-frequency side of the 1368 cm^{-1} band. As the ν_{15} mode (1351 cm^{-1}) is calculated much weak in Raman intensity, we assign the observed 1381 and 1358 cm^{-1} bands to ν_{14} and ν_{14}', both of which involves the in-plane stretching of C9C10/C5C6/C8C9 bonds. The weak or shoulder bands at 1289, 1276, 1215, 1208, 1158, and 1146 cm^{-1} are assigned to the ν_{16}, ν_{17}, ν_{18}, ν_{23}, ν_{19}'/ν_{19}, and ν_{20}'/ν_{20} modes. Most of these modes are due to the in-plane CCH bending of the naphthyl groups, with exception of ν_{23} that is dominated with C1−C1 stretching between two naphthyl groups. The strong Raman band at 1024 cm^{-1} is calculated at 1026 cm^{-1} (ν_{22}). This mode also involves in-plane CCH bending, but it contains a significant contribution of in-plane deformation of the naphthyl rings.

Our DFT calculations manifest that the non-resonance Raman band in the 400−950 cm^{-1} region is mainly due to the in-plane deformations of naphthyl ring. The observed weak Raman band at 960 cm^{-1} was calculated at 945 cm^{-1} and is assigned to in-plane deformation ν_{24} mixed slightly with out-of-plane deformation γ_3. The observed 852 cm^{-1} band of BINAM is assigned to ν_{25}, a naphthyl in-plane deformation mode involving largely the changes of the C3C4C10/C6C7C8/C5C6C7 bond-angles. DFT calculations predict this band to appear at 844 cm^{-1}, with a pretty strong Raman intensity. Two weak bands at 794 and 774 cm^{-1} were detected in the normal Raman spectrum. Based on matching of calculated and observed frequencies and intensities, we assign them to the calculated bands at 787 and 768 cm^{-1}. According to the DFT-calculations, these two modes belong to B symmetry and correspond to the in-plane skeleton deformations mixed with the C−H out-of-plane wagging of the naphthyl rings. DFT calculation for BINAM predicts a rather strong Raman band at 665 cm^{-1}. It can be readily assigned to the observed middle-strong band at 668 cm^{-1}. The calculated Cartesian atomic displacements of this mode suggest it to be ν_{27}, the in-pane deformation of the naphthyl ring mainly involving the bending of C7C8C9/C10C5C6 bond angles.

In the low-frequency region, two strong Raman band was observed at 577 and 528 cm^{-1}, respectively. We assign 528 cm^{-1} band to ν_{28}, the in-plane naphthyl deformation mainly involving the translational separation of two benzo rings of naphthyl, which is calculated at 530 cm^{-1}. In the calculated Raman spectrum, a moderately strong band was predicted at 577 cm^{-1}, which, according to the calculated atomic Cartesian displaces, can be assigned to the out-of-plane deformation of the naphthyl ring γ_9 mixed mildly with in-plane vibration like ν_{29}. Another low-frequency Raman band observed at 436 cm^{-1} is thought corresponding to the calculated band at 433 cm^{-1}, which can be assigned to the in-plane deformation of the naphthyl ring ν_{30}' combined with a γ_9'-like out-of-plane deformation.

According to our calculation, the most of the strong bands observed in non-resonance Raman belong to A symmetry, with the exceptions of the 1358 cm^{-1} band that belongs to B symmetry and the 1618 cm^{-1} band that is composed of two modes belong to A and B symmetries respectively.

3. UV resonant Raman (UVRR) spectrum excited at 325 nm

Figure 5(a) displays the resonance Raman spectrum (RRS) of BINAM excited with UV light at 325 nm, where the wavelength of the incident light is nearly in resonance with the electronic absorptions of BINAM at 348 nm. As shown in Fig.5(a), evident RR bands were observed at 1618, 1595, 1567, 1475, 1438, 1380, 1358, 1289, 1277, 1213, 1158, 1147, 1024, 851, 668,

DOI:10.1063/1674-0068/30/cjcp1606118

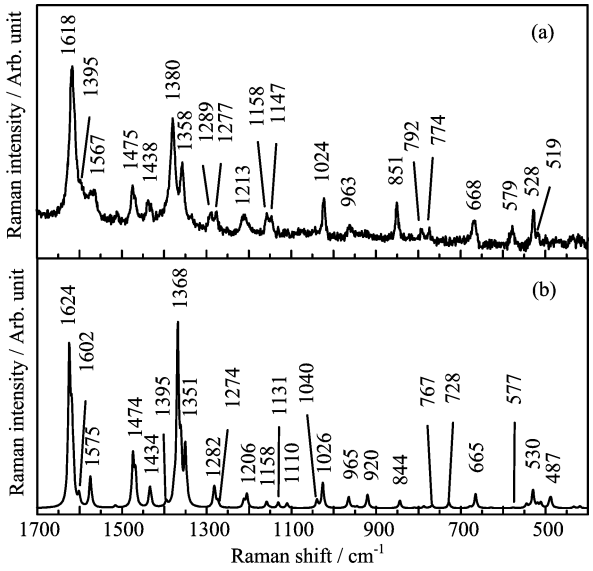

FIG. 5 UV near-resonance Raman scattering spectra of BINAM (a) experimental with the excitation wavelength λ_{ex}=325 nm, (b) calculated with CPHF-B3LYP/6-311++G(d,p).

579, and 528 cm^{-1}, most of which also appear in the 488 nm excited normal Raman with considerably intensities. However, in comparison with the normal Raman (Fig.4(a)), the RR bands at 1618, 1475, 1358, 1289, 1158 cm^{-1} show clear increase in relative intensities. Especially, the RR band 1618 cm^{-1} displays greatly enhancement, which is even stronger than the 1380 cm^{-1} band, the strongest band in normal Raman.

Theoretical simulation of UV-resonance Raman spectrum (Fig.5(b)) was carried out with frequency-dependent polarizability using coupled-perturbation theory. Experimentally, the resonance Raman spectrum was recorded by using the 325 nm line of a He-Cd laser as the excitation source, which is blue-shifted by 2034 cm^{-1} (0.252 eV) from the UV absorption band (348 nm). This energy difference must be considered in calculation model since it is known that the resonance Raman intensities sensitively depend on the wavelength difference between the incident laser line and the electronic absorption maximum. Therefore, the energy of the incident light was set as 4.01 eV, blue shifted by 0.252 eV with respect to the TDDFT calculated UV-absorption peak, for theoretical simulation of UVRR. As shown in Fig.5, the calculations well reproduce the enhancement pattern of UV near-resonance Raman spectrum. It is noticed that the calculations predicted increased relative intensities for the 1624, 1474, 1351, 1282, 1158 cm^{-1} bands of the UVRR spectrum (Fig.5(b)) as compared with theoretical normal Raman (Fig.4(b). This is consistent with the experiment observations that the corresponding bands (1618, 1475, 1358, 1289, 1158 cm^{-1}) are enhanced in 325 nm excited spectrum (Fig.5(a)) as compared with 488 nm excited one (Fig.4(a)). Especially, the 1624 cm^{-1} band was predicted to be significantly enhanced by UV excitation. Meanwhile, the 1381 cm^{-1} band remains as one of the strongest bands, which is also consistent with the experiment. According to the calculations, the 1624 cm^{-1} band in the Raman spectrum is composed of two modes, *i.e.*, 1625 cm^{-1} (ν_7+NH_2 scissoring) and 1624 cm^{-1} (ν_7'+NH_2 scissoring), and their intensity ratio is about 1:2.1. Thus one can reasonably considered that the intensity of the 1618 cm^{-1} band in Fig.5(a) comes mainly from the B symmetric γ_7' mode (with mixing of NH_2 scissoring). The enhancement pattern of UV resonant Raman of BINAM may result from both the non-zero Franck-Condon overlap due to excited state pseudo-Jahn-Teller distortion and the vibronic coupling between the excited states, which are discussed in the next section.

IV. DISCUSSION

Resonance Raman is much different from normal non-resonance Raman in physical mechanisms. For resonance Raman in which the incident irradiation is resonant with an electronic transition, Raman signals can be enhanced either due to the non-zero Frank-Condon overlap between the ground and the resonant excited state (A-term mechanism) or due to the vibronic coupling between the electronic states (B-term mechanism) [41−45]. Unless the vibrational wave functions are non-orthogonal, the vibrational overlap integrals are zero and the A-term mechanism dose not contribute Raman intensities. For any vibrational mode of a molecule, non-orthogonality of these wave functions will subsist if, between the ground state and excited states, there is either a displacement of the potential energy minimum along the normal coordinate, or a difference of vibrational frequency, *i.e.* a change in shape of the potential energy surface. Symmetry arguments indicate that such a displacement may only occur for totally symmetric modes unless the molecular symmetry is altered in the excited state. However, if a change of molecular symmetry accompanies the electronic transition, this restriction is relieved. In this case, Raman bands attributed to non-totally symmetric fundamentals may acquire intensity under resonance conditions from either the A- or B-terms of the Raman polarizability. Nevertheless, it is generally the case that the A-term contribution is much more important for totally symmetric fundamentals when the incident radiation is in resonance with a strong electric-dipole-allowed electronic transition. The domination of the totally symmetric modes (A modes) in the UVRR of BINAM, as manifested by the strong intensities of 1380, 1475, 1024, 851, 668, and 528 cm^{-1} bands in Fig.5(a), may be considered as the consequence of A-term enhancement.

In Fig.5(a), several non-totally symmetric modes (B modes), such as the 1618, 1358, 1289, and 1158 cm^{-1}

DOI:10.1063/1674-0068/30/cjcp1606118

bands, were also measured with appreciable intensities. Clark and Dines [42] have pointed out that RR bands attributed to non-totally symmetric fundamental vibrations may acquire intensity via three mechanisms: (i) A-term activity due to a change of molecular symmetry in the resonant electronic state; (ii) A-term activity due to excited-state Jahn-Teller distortion; (iii) B-term scattering, involving the vibronic coupling of the resonant state to a nearby electronic excited state. The mechanism (ii) can be considered as a specific case of mechanism (i), and it has been used to explain to the Q-band excited resonant Raman of the porphyrin compounds, in which the non-totally symmetric modes (B_{1g} and B_{2g}) have been found dramatically enhanced due to the excited state Jahn-Teller distortion [46, 47]. We consider that both the mechanisms (i) and (iii) are responsible for the enhancement of the non-totally symmetric modes in the UVRR of BINAM for the following reasons.

Firstly, as mentioned above, the broad 348 nm band in the UV absorption spectrum of BINAM can be attributed to the overlap of three electronic transitions, *i.e.*, 1^1B, 2^1B, and 2^1A. These transitions correspond to the electronic excitation from HOMO, HOMO−1 to LUMO, LUMO+1. The orbital energies of HOMO−2, HOMO−1, HOMO, LUMO, LUMO+1, LUMO+2 are −6.354, −5.540, −5.492, −1.253, −1.179, −0.428 eV, respectively, indicating that the four frontier molecular orbitals, *i.e.*, HOMO, HOMO−1 to LUMO, LUMO+1, are well separated from other orbitals. Moreover, the HOMO/HOMO−1 and LUMO/LUMO+1 are nearly degenerate, which hints a pseudo-Jahn-Teller distortion may occur for the electronic configurations $(37b)^1(39a)^1$ and $(38a)^1(38b)^1$. Under this circumstance, the two configurations, $(37b)^1(39a)^1$ and $(38a)^1(38b)^1$, can be effectively coupled by certain non-totally symmetric modes. If a molecule undergoes a change of symmetry upon excitation then the A-term active modes are those that are totally symmetric in the subgroup formed by the symmetry operations common to the ground- and excited-state point groups (common group). The B modes of BINAM, while they are non-totally symmetric under the ground state point group (C_2 group), are totally symmetric under the distorted C_1 group at the excited states. Accordingly, these modes can be enhanced via the A-term mechanism.

Secondly, non-totally symmetric modes (B modes of BINAM) can be enhanced via the B-term mechanism. According to Ref.[42], the B-term of Raman polarizability is proportional to the vibronic coupling integral between two excited states ($|e\rangle$ and $|s\rangle$), $h_{se}=\left\langle e \left| \frac{\partial H}{\partial Q} \right| s \right\rangle_0$, and inversely proportional to the energy difference of these states ($\nu_e - \nu_s$). In our UVRR experiment, the excitation line (325 nm) locates at high energy side of the main absorption band (348 nm). From TDDFT calculated excitation energies and oscillator strengths (see Table III), one may reasonably assumed that the 2^1A and 2^1B states are favorably in resonance with incident light. Symmetry argument leads to non-zero vibronic coupling between 2^1A and 2^1B states via B-modes. Moreover, the energy difference between this two states is quite small (0.0208 eV according to TD-B3LYP/6-311++G(d,p)). Therefore, both requirements for the B-term contributions to Raman intensities are satisfied for the B-modes of BINAM.

Furthermore, the dramatic enhancement for the 1618 cm^{-1} (experimental) band may be intuitively understood by the general empirical rule that the vibrational coordinates responsible for converting a molecule from its ground state equilibrium conformation to the excited-state geometry will give rise to resonance-enhanced Raman bands (Tsuboi's rule) [48]. For BINAM, the lone pair of NH_2 group can interact with the naphthyl π-system through hyper-conjugation. The electronic excitations from the ground to the 1^1B and 2^1B states induce an obvious redistribution of electron density for the NH_2 groups and the naphthyl rings, which can result in large changes for the C−N bond distances and the NH_2 bong-angles. Our DFT calculation manifests that the 1624 cm^{-1} (calculated) mode contains a significant contribution from the NH_2 bending and a moderate one from C−N stretching, thus according to Tsuboi's rule, 1624 cm^{-1} band is resonantly enhanced with the UV excitation.

V. CONCLUSION

We have studied the IR absorption, visible excited normal Raman, and UV-excited near-resonance Raman spectra of 1,1′-binaphthyl-2,2′-diamine (BINAM). Density functional theory (DFT) calculations were carried out to study the vibrational frequencies and the ground-state structure of BINAM. The measured IR and Raman spectra of BINAM were found in good accordance with the calculations. The assignments of observed IR and Raman bands were proposed on the basis of the calculated and measured frequencies and intensities. In comparison with the visible excited normal Raman, several bands of BINAM were found dramatically enhanced in the UV resonance Raman spectrum. Possible excited state structure distortion was discussed based on the RR intensity analyses.

Supplementary materials: Atomic cartesian displacements for the normal modes of 1-chloro-2-naphthylamine are shown.

VI. ACKNOWLEDGMENTS

This work was supported by the National Natural Science Foundation of China (No.21273211, No.21573208), USTC-NSRL Association Foundation (No.NSRLLHJJ(14-15-012), and the Supercomputation Center of USTC.

DOI:10.1063/1674-0068/30/cjcp1606118

[1] L. Pu, Chem. Rev. **98**, 2405 (1998).
[2] Y. Chen, S. Yekta, and A. K. Yudin, Chem. Rev. **103**, 3155 (2003).
[3] N. Yoshikawa, Y. M. A. Yamada, J. Das, H. Sasai, and M. Shibasaki, J. Am. Chem. Soc. **121**, 4168 (1999).
[4] J. R. Robinson, X. Fan, J. Yadav, P. J. Carroll, A. J. Wooten, M. A. Pericas, E. J. Schelter, and P. J. Walsh, J. Am. Chem. Soc. **136**, 8034 (2014).
[5] Y. Shibata and M. Yamanaka, J. Org. Chem. **78**, 3731 (2013).
[6] M. N. Grayson, S. C. Pellegrinet, and J. M. Goodman, J. Am. Chem. Soc. **134**, 2716 (2012).
[7] N. Takenaka, Y. Huang, and V. H. Rawal, Tetrahedron **58**, 8299 (2002).
[8] G. Guillena, M. del C. Hita, C. Nájera, and S. F. Viózquez, J. Org. Chem. **73**, 5933 (2008).
[9] G. Guillena, M. del C. Hita, C. Nájera, and S. F. Viózquez, Tetrahedron: Asymmetry **18**, 2300 (2007).
[10] G. Guillena, M. del C. Hita, and C. Nájera, Tetrahedron: Asymm. **17**, 1493 (2006).
[11] G. Guillena, M. del C. Hita, and C. Nájera, Tetrahedron: Asymm. **17**, 729 (2006).
[12] A. Bañón-Caballero, G. Guillena, and C. Nájera, Green Chem. **12**, 1599 (2010).
[13] W. L. Duan, M. Shi, and G. B. Rong, Chem. Commun. 2916 (2003).
[14] A. R. Chianese and R. H. Crabtree, Organometallics **24**, 4432 (2005).
[15] H. M. Nelson, J. S. Patel, H. P. Shunatona, and F. D. Toste, Chem. Sci. **6**, 170 (2015).
[16] Q. Xu, X. Gu, S. Liu, Q. Dou, and M. Shi, J. Org. Chem. **72**, 2240 (2007).
[17] B. Tan, N. R. Candeias, and C. F. Barbas III, Nat. Chem. **3**, 473 (2011).
[18] S. N. Sluijter, L. J. Jongkind, and C. J. Elsevier, Eur. J. Inorg. Chem. 2948 (2015).
[19] H. I. S. Nogueira and S. M. O. Quintal, Spectrochim. Acta A **56**, 959 (2000).
[20] V. Setnička, M. Urbanová, P. Bouř, V. Král, and K. Volka, J. Phys. Chem. A **105**, 8931 (2001).
[21] C. F. Chang, S. C. Wang, and S. Shigeto, J. Phys. Chem. C **118**, 2702 (2014).
[22] Z. Y. Li, D. M. Chen, T. J. He, and F. C. Liu, J. Phys. Chem. A **111**, 4767 (2007).
[23] S. Fujiyoshi, S. Takeuchi, and T. Tahara, J. Phys. Chem. A **108**, 5938 (2004).
[24] K. Takaishi, J. Suzuki, T. Yabe, H. Asano, M. Nishikawa, D. Hashizume, A. Muranaka, M. Uchiyama, and A. Yokoyama, Org. Lett. **17**, 4098 (2015).
[25] L. G. Da, T. T. Lu, M. Xiang, T. J. He, and D. M. Chen, Chin. J. Chem. Phys. **21**, 367 (2008).
[26] M. A. Belkin, S. H. Han, X. Wei, and Y. R. Shen, Phys. Rev. Lett. **87**, 113001 (2001).
[27] N. Ji, V. Ostroverkhov, M. A. Belkin, Y. J. Shiu, and Y. R. Shen, J. Am. Chem. Soc. **128**, 8845 (2006).
[28] M. A. Belkin and Y. R Shen, Phys. Rev. Lett. **91**, 213907 (2003).
[29] R. H. Zheng, D. M. Chen, W. M. Wei, T. J. He, and F. C. Liu, J. Phys. Chem. B **110**, 4480 (2006).
[30] R. H. Zheng, W. M. Wei, Y. Y. Jing, H. Liu, and Q. Shi, J. Phys. Chem. C **117**, 11117 (2013).
[31] V. Liégeois, ChemPhysChem **10**, 2017 (2009).
[32] A. D. Becke, J. Chem. Phys. **98**, 5648 (1993).
[33] C. Lee, W. Yang, and R. G. Parr, Phys. Rev. B **37**, 785 (1988).
[34] R. E. Oakes, S. J. Spence, and S. E. J. Bell, J. Phys. Chem. A **107**, 2964 (2003).
[35] A. P. Scott and L. Radom, J. Phys. Chem. **100**, 16502 (1996).
[36] R. Bauernschmitt and R. Ahlrichs, Chem. Phys. Lett. **256**, 454 (1996).
[37] M. E. Casida, C. Jamorski, K. C. Casida, and D. R. Salahub, J. Chem. Phys. **108**, 4439 (1998).
[38] R. E. Stratmann, G. E. Scuseria, and M. J. Frisch, J. Chem. Phys. **109**, 8218 (1998).
[39] M. J. Frisch, G. W. Trucks, H. B. Schlegel, G. E. Scuseria, M. A. Robb, J. R. Cheeseman, G. Scalmani, V. Barone, B. Mennucci, G. A. Petersson, H. Nakatsuji, M. Caricato, X. Li, H. P. Hratchian, A. F. Izmaylov, J. Bloino, G. Zheng, J. L. Sonnenberg, M. Hada, M. Ehara, K. Toyota, R. Fukuda, J. Hasegawa, M. Ishida, T. Nakajima, Y. Honda, O. Kitao, H. Nakai, T. Vreven, J. A. Montgomery, Jr., J. E. Peralta, F. Ogliaro, M. Bearpark, J. J. Heyd, E. Brothers, K. N. Kudin, V. N. Staroverov, T. Keith, R. Kobayashi, J. Normand, K. Raghavachari, A. Rendell, J. C. Burant, S. S. Iyengar, J. Tomasi, M. Cossi, N. Rega, J. M. Millam, M. Klene, J. E. Knox, J. B. Cross, V. Bakken, C. Adamo, J. Jaramillo, R. Gomperts, R. E. Stratmann, O. Yazyev, A. J. Austin, R. Cammi, C. Pomelli, J. W. Ochterski, R. L. Martin, K. Morokuma, V. G. Zakrzewski, G. A. Voth, P. Salvador, J. J. Dannenberg, S. Dapprich, A. D. Daniels, O. Farkas, J. B. Foresman, J. V. Ortiz, J. Cioslowski, and D. J. Fox, *Gaussian 09, Revision D.01*, Wallingford CT: Gaussian, Inc., (2013).
[40] J. R. Scherer, J. Chem. Phys. **36**, 3308 (1962).
[41] B. B. Johnson and W. L. Peticolas, Annu. Rev. Phys. Chem. **27**, 465 (1976).
[42] R. J. H. Clark and T. J. Dines, Angew. Chem Int. Ed. Engl. **25**, 131 (1986).
[43] S. Hassing and O. S. Mortensen, J. Mol. Spectrosc. **87**, 1 (1981).
[44] I. Tehver, H. Kaasik, and V. Hizhnyakov, J. Raman Spectrosc. **33**, 639 (2002).
[45] H. Torii, M. Tasumi, I. M. Bell, and R. J. H. Clark, Chem. Phys. **216**, 67 (1997).
[46] J. A. Shelnutt, L. D. Cheung, R. C. C. Chang, N. T. Yu, and R. H. Felton, J. Chem. Phys. **66**, 3387 (1977).
[47] L. D. Cheung, N. T. Yu, and R. H. Felton, Chem. Phys. Lett. **55**, 527 (1978).
[48] A. Y. Hirakawa and M. Tsuboi, Science **188**, 359 (1975).

DOI:10.1063/1674-0068/30/cjcp1606118